

Resonator–zero-qubit architecture for superconducting qubitsAndrei Galiutdinov,^{1,*} Alexander N. Korotkov,^{1,†} and John M. Martinis²¹*Department of Electrical Engineering, University of California, Riverside, California 92521, USA*²*Department of Physics, University of California, Santa Barbara, California 93106, USA*

(Received 19 May 2011; revised manuscript received 8 February 2012; published 23 April 2012)

We analyze the performance of the resonator–zero-qubit (RezQu) architecture in which the qubits are complemented by memory resonators and coupled via a resonator bus. Separating the stored information from the rest of the processing circuit by at least two coupling steps and the zero qubit state results in a significant increase in the on-to-off ratio and a reduction in the idling error. Assuming no decoherence, we calculate such idling error, as well as the errors for the MOVE operation and tunneling measurement, and show that the RezQu architecture can provide the high-fidelity performance required for medium-scale quantum information processing.

DOI: [10.1103/PhysRevA.85.042321](https://doi.org/10.1103/PhysRevA.85.042321)

PACS number(s): 03.67.Lx, 85.25.–j

I. INTRODUCTION

Superconducting circuits with Josephson junctions are steadily gaining attention as promising candidates for the realization of a quantum computer [1]. Over the last several years, significant progress has been made in preparing, controlling, and measuring the macroscopic quantum states of such circuits [2–12]. However, the two major roadblocks—scalability and decoherence—remain, impeding the development of a workable prototype. The resonator–zero-qubit (RezQu) protocol presented here aims to address these limitations at a low-level (hardware cell) architecture [13].

A RezQu device consists of a set of superconducting qubits (e.g., phase qubits [14]), each of which is capacitively coupled to its own memory resonator and also capacitively coupled to a common resonator bus, as shown in Fig. 1 [7,15–17]. The bus is used for coupling operations between qubits, while the memory resonators are used for information storage when the logic qubits are idling. With the coupling capacitors being fixed and relatively small, qubit coupling is adjusted by varying the qubit frequency, which is brought in and out of resonance with the two resonators. For a one-qubit operation, quantum information is moved from the memory to the qubit, where a microwave pulse is applied. A natural two-qubit operation is the controlled- Z gate, for which one qubit state is moved to the bus, while the other qubit frequency is tuned close to resonance with the bus for a precise duration [6,18–20].

Most importantly, the information stored in resonators is separated from the rest of the processing circuit by the known qubit state $|0\rangle$ and at least two coupling steps, thus reducing crosstalk error during idling. Also, the problem of spectral crowding is essentially eliminated because the two-step resonance between empty qubits is not harmful, while the four-step coupling between memory resonators is negligible. Therefore the resonator frequencies, which are set by fabrication, can be close to each other, decreasing sensitivity to phase errors in the clock. Thus the RezQu architecture essentially solves the inherent on-to-off ratio problem of the *fixed* capacitive coupling without using the more complicated

scheme of a tunable coupling [8,21,22]. As an additional benefit, information storage in resonators increases coherence time compared to storage in the qubits. We note that the idea of using resonators to couple qubits has been suggested by many authors [23–32]. The use of resonators as quantum memories has also been proposed previously [31,33–35]. However, putting the two ideas together in a single architecture results in new qualitative advantages, which have not been discussed.

In this paper we briefly consider the relation between the logical and the physical qubit states and then analyze several basic operations in the RezQu architecture. In particular, for a truncated three-component memory-qubit-bus RezQu device, we focus on the idling error, information transfer (MOVE) between the qubit and its memory, and the tunneling measurement. The analysis of the controlled- Z gate will be presented elsewhere [36]. For simplicity, decoherence is neglected.

II. LOGICAL VS PHYSICAL QUBITS

We begin by recalling an important difference between logical and actual, physical qubits. The difference stems from the fact that in the language of quantum circuit diagrams the idling qubits are always presumed to be stationary [37], while superconducting qubits evolve with a 4- to 10-GHz frequency even in idling, which leads to accumulation of relative phases. Also, the always-on coupling leads to fast small-amplitude oscillations of the “bare”-state populations during off-resonant idling. A natural way to avoid the latter problem is to *define* logical multiqubit states to be the (dressed) *eigenstates* of the whole system (see, e.g., [5,26,28,29,38,39] for discussion of the dressed states). Then the only evolution in idling is the phase accumulation for each logic state. However, there are 2^N logic states for N qubits, and using 2^N “local clocks” (rotating frames) would require an exponential overhead to calibrate the phases. The present-day experiments with two or three qubits often use this unscalable way, but it will not work for $N \gtrsim 10$. A scalable way is to choose only N rotating frames, which correspond to one-qubit logical states, and treat the frequencies of multiqubit states only approximately, as sums of the corresponding single-qubit frequencies. The use of such nonexact rotating frames for multiqubit states leads to what we call an idling error, which is analyzed in the next section.

*Present address: Department of Physics and Astronomy, University of Georgia, Athens, GA 30602; ag@physast.uga.edu

†korotkov@ee.ucr.edu

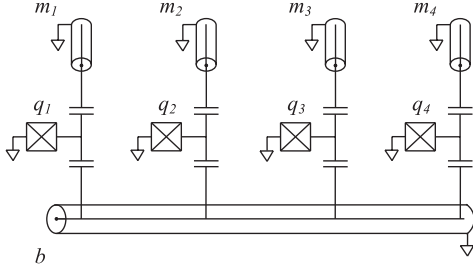


FIG. 1. Schematic diagram of the RezQu architecture: m , memory resonators; q , qubits; b , bus. We assume frequencies of ~ 7 GHz for the memories and ~ 6 GHz for the bus, and qubit frequencies are varied between these values.

Note that it is sufficient to establish a correspondence between logical and physical states only at some moments between the gates. Moreover, this correspondence may be different at different moments. At those moments, the bus is empty, the $2N + 1$ system components (N qubits, N memories, and the bus) are well detuned from their neighbors, and for each logical qubit it is unambiguously known whether the corresponding quantum information is located in the memory or in the qubit. Thus the eigenstates corresponding to the logical states are well defined and the physical-to-logical correspondence is naturally established by projecting onto the 2^N computational eigenstates, while occupations of other eigenstates should be regarded as an error. In the simplest modular construction of an algorithm we should not attempt to correct the error of a given gate by the subsequent gates. Then for the overall error we only need to characterize the errors of individual gates, as well as the idling error.

One may think that defining logical states via the eigenstates of the whole system may present a technical problem in an algorithm design. However, this is not really a problem, for the following reasons. First, we need the conversion into the basis of eigenstates only at the start and end of a quantum gate, while the design of a gate is modular and can be done using any convenient basis. Second, in practice, we can truncate the system to calculate the eigenstates approximately, making sure that the error due to truncation is sufficiently small. Similar truncation with a limited error is needed in practical gate design.

As mentioned above, the physical-to-logical correspondence rule can be different at every point between the gates. For the correspondence based on eigenstates we are free to choose N single-excitation phases arbitrarily. Despite this freedom, for definiteness, it makes sense to relate all the single-excitation phases to a particular fixed time moment in an algorithm. Then a shift of the gate start time leads to easily calculable phase shifts, which accumulate with frequencies equal to the change in single-excitation frequencies before and after the gate. Such shift is useful for the adjustment of relative single-excitation phases [40]. Another way of the single-excitation phase adjustment is by using “qubit frequency excursions” [7]. The ease of these adjustments significantly simplifies design of quantum gates, because we essentially should not worry about the single-excitation phases.

Note that the initial generation of high-fidelity single-excitation eigenstates is much easier experimentally than the generation of bare states. This is because the typical duration of qubit excitation pulses is significantly longer than the inverse detuning between the qubit and the resonators. We have checked this advantage of using eigenstates versus bare states numerically in a simple model with typical parameters [7] of a RezQu device (the error decrease is about 2 orders of magnitude). Similarly, the standard one-qubit operations essentially operate with the eigenstates rather than with the bare states.

III. IDLING ERROR

Before discussing the idling error in the RezQu architecture, let us consider a simpler case of two directly coupled qubits. Then in idling the wave function evolves as $|\psi(t)\rangle = \alpha_{00}e^{-i\epsilon_{00}t}|\overline{00}\rangle + \alpha_{01}e^{-i\epsilon_{01}t}|\overline{01}\rangle + \alpha_{10}e^{-i\epsilon_{10}t}|\overline{10}\rangle + \alpha_{11}e^{-i\epsilon_{11}t}|\overline{11}\rangle$, where we denote the logical (eigen)states with an overline, their corresponding (eigen)energies by ϵ_{ij} , and amplitudes at $t = 0$ by α_{ij} . However, for the desired evolution $|\psi^{\text{desired}}(t)\rangle$ the last term should be replaced with $\alpha_{11}e^{-i(\epsilon_{01} + \epsilon_{10} - \epsilon_{00})t}|\overline{11}\rangle$; then only two rotating frames (clocks), with frequencies $\epsilon_{01} - \epsilon_{00}$ and $\epsilon_{10} - \epsilon_{00}$, are needed. We see that the phase difference accumulates with the frequency $\Omega_{ZZ} = (\epsilon_{11} - \epsilon_{01}) - (\epsilon_{10} - \epsilon_{00})$, and therefore the idling error \mathcal{E} due to qubit coupling accumulates over a time t as

$$\mathcal{E} = 1 - |\langle \psi^{\text{desired}}(t) | \psi(t) \rangle|^2 \simeq |\alpha_{11}|^2 (1 - |\alpha_{11}|^2) (\Omega_{ZZ} t)^2 \lesssim (\Omega_{ZZ} t)^2, \quad (1)$$

where we have assumed $\Omega_{ZZ} t \ll 1$. (The frequency Ω_{ZZ} is defined in the same way as in Ref. [39] for a two-qubit $\sigma_Z^{(1)} \sigma_Z^{(2)}$ interaction.) The error is state dependent, but in this paper we always consider error estimates for the worst-case scenario.

In the RezQu architecture, the main contribution to the idling error comes from interaction between a memory resonator, in which quantum information is stored, and the bus, which is constantly used for quantum gates between other qubits. By analogy with the above case, for the truncated memory-qubit-bus (mqb) system the idling error can be estimated as

$$\mathcal{E} \simeq (\Omega_{ZZ} t)^2, \quad \Omega_{ZZ} = (\epsilon_{101} - \epsilon_{001}) - (\epsilon_{100} - \epsilon_{000}), \quad (2)$$

where the eigenenergies correspond to the logical eigenstates $|\overline{101}\rangle$, $|\overline{001}\rangle$, $|\overline{100}\rangle$, $|\overline{000}\rangle$, and in our $|\overline{mqb}\rangle$ notation the sequence of symbols represents the states of the memory resonator, the qubit, and the bus. Note that the qubit here is always in state $|0\rangle$, and Ω_{ZZ} is essentially the difference in the effective frequencies of the memory resonator in the presence vs the absence of bus excitation.

To find Ω_{ZZ} we use the rotating-wave approximation (RWA); then the dynamics of the mqb system is described by the Hamiltonian (we use $\hbar = 1$)

$$H(t) = \begin{bmatrix} 0 & 0 & 0 \\ 0 & \omega_q(t) & 0 \\ 0 & 0 & 2\omega_q(t) - \eta \end{bmatrix} + \omega_m a_m^\dagger a_m + \omega_b a_b^\dagger a_b + g_m (a_m^\dagger \sigma_q^- + a_m \sigma_q^+) + g_b (\sigma_q^- a_b^\dagger + \sigma_q^+ a_b) + g_d (a_m^\dagger a_b + a_m a_b^\dagger), \quad (3)$$

where the qubit frequency ω_q may vary in time, while the qubit anharmonicity η is assumed to be constant;

$$\sigma_q^- = \begin{bmatrix} 0 & 1 & 0 \\ 0 & 0 & \sqrt{2} \\ 0 & 0 & 0 \end{bmatrix}, \quad \sigma_q^+ = (\sigma_q^-)^\dagger \quad (4)$$

are the qubit lowering and raising operators; ω_m and ω_b are the memory and the bus frequencies (which are presumed to be fixed); a_m^\dagger , a_m , a_b^\dagger , and a_b are the creation and annihilation operators for the memory and the bus photons; and g_m and g_b are the memory-qubit and qubit-bus coupling constants. The last term in Eq. (3) describes the direct (electrostatic) memory-bus coupling; replacing a qubit in Fig. 1 with a lumped tank circuit, it is found [41] to be

$$g_d = 2g_m g_b / \omega_q. \quad (5)$$

It is typically smaller than the effective memory-bus coupling via the virtual excitation of the qubit because the detunings $|\omega_m - \omega_q|$ and $|\omega_b - \omega_q|$ between the elements are much smaller than their frequencies; because of that, we often neglect g_d . From the physical model it is easy to show that g_m and g_b are proportional to $\omega_q^{1/2}$ and therefore change when the qubit frequency is varied; however, for simplicity we assume constant g_m and g_b .

Neglecting g_d , in fourth order we find (see the Appendix),

$$\Omega_{ZZ} = \frac{-2g_m^2 g_b^2 \eta}{\Delta_m^2 \Delta_b^2} \frac{\omega_m + \omega_b - 2\omega_q}{\omega_m + \omega_b - (2\omega_q - \eta)}, \quad (6)$$

$$\Delta_m = \omega_m - \omega_q, \quad \Delta_b = \omega_q - \omega_b, \quad (7)$$

which is very close to the exact value found by direct diagonalization of the Hamiltonian (Fig. 2), and the effect of g_d is of a higher order and therefore very small (see the Appendix

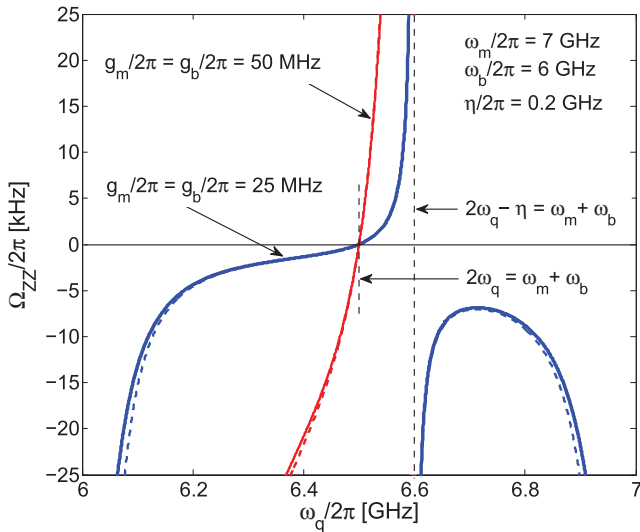


FIG. 2. (Color online) Frequency Ω_{ZZ} for a truncated memory-qubit-bus system [the idling error is $(\Omega_{ZZ}t)^2$] for two values of the coupling: $g_m/2\pi = g_b/2\pi = 25$ MHz (blue lines) and $g_m/2\pi = g_b/2\pi = 50$ MHz (red lines). Solid lines show the results of exact diagonalization of the RWA Hamiltonian, (3), with and without g_d . The effect of g_d is not visible (smaller than the line thickness). Blue and red dashed lines show the analytical result, (6).

and Fig. 2). Note that $\Omega_{ZZ} \propto \eta$ because in a linear system $\Omega_{ZZ} = 0$, and nonlinearity comes from the qubit. Equation (6) shows that an optimal choice of the qubit “parked” frequency is $\omega_q = (\omega_m + \omega_b)/2$, midway between the memory and the bus frequencies; then the idling error in this order goes to zero (this happens because the contribution of $|020\rangle$ in $|101\rangle$ becomes zero; see the Appendix). Note that in the RezQu architecture the frequencies of the memory resonators are assumed to be relatively close to each other (forming a “memory band” of frequencies). Then the optimal parked frequencies of the qubits are also close to each other. This is not a problem when all qubits are in state $|0\rangle$; however, when a qubit is excited this may lead to a significant resonant coupling with another qubit via the bus. To avoid this “spectral crowding” effect, it is useful to reserve two additional frequencies, situated sufficiently far from the parked frequencies, at which a pair of qubits may undergo local rotations (simultaneous rotations of two qubits are often useful before and after two-qubit gates).

The idling error, (2), scales quadratically with time. This is because we use a definition for which not the error itself but its square root corresponds to a metric, and therefore for a composition of quantum gates, in the worst-case scenario we should sum square roots of the errors [37]. For the same reason, the worst-case idling error scales quadratically, $\mathcal{E} \propto N^2$, with the number N of qubits in a RezQu device. In principle, an average idling error may scale linearly with N and time (for that we would need to define the memory “clock” frequency using an average occupation of the bus); however, here we use only the worst-case analysis.

It is convenient to replace the time dependence in the idling error estimate $(N\Omega_{ZZ}t)^2$ with the dependence on the number of operations N_{op} in an algorithm. (The corresponding quadratic dependence on N_{op} can also be interpreted as the worst-case-scenario error for a composition of quantum operations.) Assuming that each operation crudely takes time $t_{\text{op}} \simeq g_m^{-1} + g_b^{-1}$ (this estimate comes from MOVE operations discussed later and also from the controlled-Z gate) and neglecting the second factor in Eq. (6) (i.e., assuming nonoptimal parked qubit frequencies), we obtain the following estimate for the worst-case idling error:

$$\mathcal{E} \simeq \frac{g_m^3 g_b^3 \eta^2 N^2 N_{\text{op}}^2}{\Delta_m^4 \Delta_b^4} \frac{\max(g_m, g_b)}{\min(g_m, g_b)}, \quad (8)$$

where Δ_m and Δ_b are typical detunings at idling. Using for an estimate $g_m/2\pi = g_b/2\pi = 25$ MHz, $\eta/2\pi = 200$ MHz, and $\Delta_m/2\pi = \Delta_b/2\pi = 500$ MHz, we obtain $\mathcal{E} \simeq 10^{-8} N^2 N_{\text{op}}^2$.

To demonstrate the advantage of the RezQu architecture, Eq. (8) may be compared with the corresponding result for the conventional bus-based architecture (without additional memories). Then the idling error is due to ZZ interaction between the qubit and the bus: the frequency of an idling qubit is affected by the bus occupation due to logic operations between other qubits. In this case $\Omega_{ZZ, \text{conv}} = -2g_b^2 \eta / [\Delta_b(\Delta_b - \eta)]$, which gives

$$\mathcal{E}_{\text{conv}} \simeq g_b^2 \eta^2 N^2 N_{\text{op}}^2 / \Delta_b^4. \quad (9)$$

Assuming a typical ratio $g/\Delta \lesssim 0.1$ between the coupling and the detuning, we have a reduction in the idling error in the RezQu architecture by at least 10^4 even before considering

that Ω_{ZZ} can be zeroed in this order. Using Eq. (9) we see that a conventional architecture allows only a very modest number of qubits and operations before the idling error becomes significant. In principle, the problem can be solved by a constantly running dynamical decoupling (which would be quite nontrivial in a multiqubit device). The RezQu idea eliminates the need for such dynamical decoupling.

All our estimates so far have been for the idling error due to the memory-bus interaction. Now let us discuss errors due to the four-step memory-memory interaction in the RezQu architecture. The XX interaction between the memory and another (k th) memory can be calculated [39] as $\Omega_{XX} = 2g_m g_{m,k} g_b g_{b,k} / [\Delta_m \Delta_{m,k} (\omega_m - \omega_b)]$, where the additional subscript k indicates parameters for the k th section of the device. The XX interaction does not produce a phase error accumulating in idling but leads to the error $\mathcal{E} \simeq (\Omega_{XX} / \delta_m)^2$ every time the information is retrieved from memory, where δ_m is the typical spacing between memory frequencies. Assuming similar sections of the RezQu device with $\Delta_b \simeq \Delta_m \equiv \Delta$ and $\delta_m \simeq \Delta / N$, we obtain an error estimate $\mathcal{E} \simeq (N g_m^2 g_b^2 / \Delta^4)^2$ per operation. Since the worst-case scaling with the number of operations N_{op} is always $\propto N_{\text{op}}^2$, we obtain the worst-case estimate

$$\mathcal{E} \simeq N^2 N_{\text{op}}^2 g_m^4 g_b^4 / \Delta^8. \quad (10)$$

This error is smaller than the idling error (8) if $g_{m,b} < \eta$. For $g_m = g_b = \Delta / 20$ we find a very small error, $\mathcal{E} \simeq 10^{-10} N^2 N_{\text{op}}^2$, which means that there is essentially no spectral crowding problem for memories. Note that for a conventional bus-based architecture the error estimate (10) is replaced with $\mathcal{E}_{\text{conv}} \simeq N^2 N_{\text{op}}^2 g_b^4 / \Delta^4$ and presents a difficult scaling problem due to the spectral crowding.

Besides the XX interaction between the two memories, there is also the ZZ interaction. Using the same approximate derivation as in the Appendix [see Eq. (A7)] and assuming $\Delta_b \simeq \Delta_m \equiv \Delta$, we find an estimate $\Omega_{ZZ} \approx -\eta g_m^4 g_b^4 / \Delta^8$. Then using $\mathcal{E} \simeq (\Omega_{ZZ} t_{\text{op}})^2 N_{\text{op}}^2 N^4$ (the scaling N^4 is because each pair brings a contribution), with $t_{\text{op}} \simeq g_m^{-1} + g_b^{-1}$, we obtain the worst-case estimate

$$\mathcal{E} \simeq \frac{g_m^7 g_b^7 \eta^2 N^4 N_{\text{op}}^2}{\Delta^{16}} \frac{\max(g_m, g_b)}{\min(g_m, g_b)}. \quad (11)$$

This error is smaller than the memory-bus idling error, (8), if $N < \Delta^4 / g_m^2 g_b^2$, which is always the case in practice.

IV. MOVE OPERATION

Any logic gate in the RezQu architecture requires moving quantum information from one system element (memory, qubit, or bus) to another. Therefore the MOVE operation is the most frequent one. It is important to mention that the one-way MOVE operation [41] is easier to design than the SWAP (or i SWAP) operation because we are not interested in the fidelity of the reverse transfer and can also assume zero occupation of the neighboring element. For example, for a perfect qubit \rightarrow memory MOVE (i MOVE) operation in the truncated mqb system, we search for a unitary, which transforms $|\overline{010}\rangle \rightarrow -i|\overline{100}\rangle$ (note that in the RWA, $|\overline{000}\rangle \rightarrow |\overline{000}\rangle$ always), but we are not interested in what happens to the initial states $|\overline{001}\rangle$ and $|\overline{100}\rangle$. Moreover, we can allow for an

arbitrary phase, $|\overline{010}\rangle \rightarrow -i e^{-i\varphi} |\overline{100}\rangle$, because this phase can be compensated either by shifting of the operation start time within one period of the initial memory-qubit detuning [40] or by ‘‘qubit frequency excursion’’ with proper integral [7]. Therefore, we need to satisfy only two (complex) equations to design the unitary U_{MOVE} for this MOVE operation,

$$\langle \overline{010} | U_{\text{MOVE}} | \overline{010} \rangle = 0, \quad \langle \overline{001} | U_{\text{MOVE}} | \overline{010} \rangle = 0. \quad (12)$$

Experimentally the qubit \rightarrow memory MOVE operation is done [7,15,16,40] by tuning the qubit in resonance (with some overshoot) with the memory resonator approximately for a duration $\pi / 2g_m$. Equation (12) means that any reasonable shape of the $\omega_q(t)$ tune/detune pulse with four adjustable parameters can be used for a perfect MOVE operation in the truncated mqb system. Actually, as discussed later, the use of only two adjustable parameters is sufficient to obtain an exponentially small error in the quasiadiabatic regime. Such a two-parameter construction is most convenient for practical purposes, but formally it is imperfect (nonzero error). So we first discuss the perfect (zero-error) four-parameter construction.

We have designed the qubit \rightarrow memory MOVE pulses $\omega_q(t)$ for the truncated mqb device both analytically (in first order) and numerically. The initial and final frequencies of the qubit are allowed to be different. In the analytical design we do calculations in the bare basis, $|\psi(t)\rangle = \alpha(t)|100\rangle + \beta(t)|010\rangle + \gamma(t)|001\rangle$, but define the comoving frame as

$$\tilde{\alpha} = \alpha e^{i\omega_m t}, \quad \tilde{\beta} = \beta e^{i \int_0^t \omega_q(t') dt'}, \quad \tilde{\gamma} = \gamma e^{i\omega_b t}. \quad (13)$$

In this representation the only interesting initial state $|\overline{010}\rangle$ of the qubit \rightarrow memory MOVE operation is (in first order)

$$\tilde{\alpha}(0) = -g_m / \Delta_m(0), \quad \tilde{\beta}(0) = 1, \quad \tilde{\gamma}(0) = g_b / \Delta_b(0), \quad (14)$$

where $\Delta_m = \omega_m - \omega_q$ and $\Delta_b = \omega_q - \omega_b$ are the detunings. The desired (target) final state at time t_f is $-i e^{-i\varphi} |\overline{100}\rangle$, i.e.,

$$\begin{aligned} \tilde{\alpha}(t_f) &= -i e^{-i\varphi}, \quad \tilde{\gamma}(t_f) = 0, \\ \tilde{\beta}(t_f) &= -i e^{-i\varphi} g_m \Delta_m^{-1}(t_f) e^{-i \int_0^{t_f} \Delta_m(t') dt'}. \end{aligned} \quad (15)$$

Note that even though the phase φ is arbitrary, the relative phase between $\tilde{\alpha}(t_f)$ and $\tilde{\beta}(t_f)$ is fixed by the absence of the relative phase between $\alpha(t_f)$ and $\beta(t_f)$. We see that the MOVE operation should eliminate the initial ‘‘tail’’ $\tilde{\gamma}(0)$ on the bus (this needs two real parameters in the pulse design) and transfer most of the excitation to the memory with the correct magnitude and relative phase of $\tilde{\beta}(t_f)$ (two more real parameters).

Similarly to the experimental pulse design [7,15,16,40], we assume that the shape of the $\omega_q(t)$ pulse consists of a front ramp, a rear ramp, and a flat part in between them (Fig. 3 illustrates a piecewise-linear construction of the pulse). As shown below, using two parameters for the front ramp shape, we can ensure elimination of the ‘‘tail’’ $\tilde{\gamma}(t_f)$; we can choose a rather arbitrary rear ramp, and using two parameters for the flat part (its frequency overshoot and duration), we can provide proper $\tilde{\beta}(t_f)$.

Let us start with the ‘‘tail’’ $\tilde{\gamma}$. As follows from the Schrödinger equation with Hamiltonian (3),

$$\tilde{\gamma}(t_f) = \tilde{\gamma}(0) - i g_b \int_0^{t_f} dt \tilde{\beta}(t) e^{-i \int_0^t \Delta_b(t') dt'}. \quad (16)$$

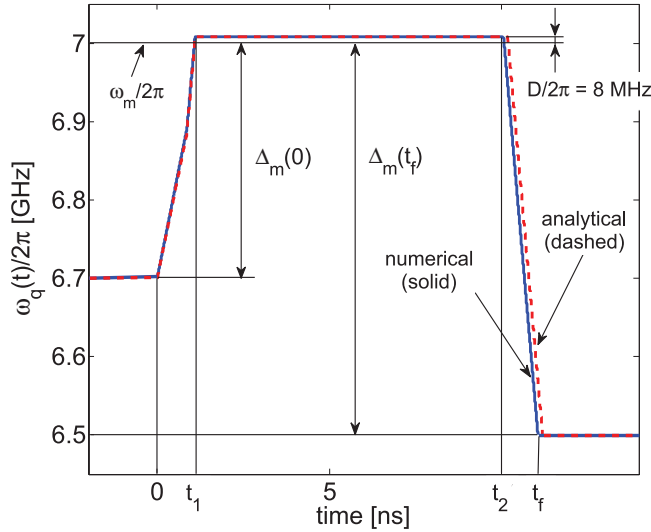


FIG. 3. (Color online) Illustration of a piecewise-linear tune/detune pulse shape (qubit frequency as a function of time) for the MOVE operation qubit \rightarrow memory in a three-component mqb system. The front ramp consists of two straight segments. The solid (blue) line shows the result of a four-parameter numerical optimization in which the slope of the first straight segment, the qubit frequency at the end of the first straight segment, the duration $t_2 - t_1$ of the flat part, and its overshoot D have been optimized. This gives $\mathcal{E} = 0$ up to machine accuracy. The dashed (red) line shows the analytical design based on Eqs. (17) and (22); in this case, $\mathcal{E} = 5 \times 10^{-4}$. System parameters: $\omega_m/2\pi = 7$ GHz, $\omega_b/2\pi = 6$ GHz, $\omega_q(0)/2\pi = 6.7$ GHz, $\omega_q(t_f)/2\pi = 6.5$ GHz, and $g_m/2\pi = g_b/2\pi = 25$ MHz. The slopes of the second front segment and of the final ramp have been fixed at 500 MHz/ns.

Let us denote the end of the front ramp t_1 and the start of the rear ramp t_2 (see Fig. 3). For $0 < t < t_1$ in Eq. (16) we can replace $\tilde{\beta}(t)$ with $\tilde{\beta}(0) = 1$ because the qubit occupation cannot change much during a short ramp. For $t_1 < t < t_2$ we can use integration by parts using $\Delta_b(t) \approx \omega_m - \omega_b$, with $\tilde{\beta}(t)$ changing approximately from 1 to 0. Finally, there is a negligible (second order in g_b) contribution to the integral for $t_2 < t < t_f$ because $\tilde{\beta}(t)$ is already small (first order in g_b). Thus for the desired pulse shape, in first order we obtain

$$0 = \frac{\tilde{\gamma}(t_f)}{g_b} = \frac{1}{\Delta_b(0)} - i \int_0^{t_1} e^{-iA'_0} dt - \frac{e^{-iA'_0}}{\omega_m - \omega_b}, \quad (17)$$

$$A'_{t'} \equiv \int_{t'}^{t''} \Delta_b(t) dt. \quad (18)$$

As we see, the required elimination of the tail $\tilde{\gamma}$ on the bus gives two equations (real and imaginary parts) for the front ramp shape. This can be done by using practically any shape with two adjustable parameters. Note that condition (17) essentially means that in order to have a correct (zero) tail on the bus at final time t_f , this tail at time t_1 should be the same as the tail for the comoving eigenstate of the qubit-bus system.

Now let us design the flat part of the pulse, which should give us the proper ratio $\tilde{\beta}(t_f)/\tilde{\alpha}(t_f)$ from Eq. (15). After designing the front ramp we know $\tilde{\alpha}$ and $\tilde{\beta}$ at the start of

the flat part t_1 : in first order, $\tilde{\beta}(t_1) = 1$ and

$$\frac{\tilde{\alpha}(t_1)}{\tilde{\beta}(t_1)} = \frac{-g_m}{\Delta_m(0)} - i g_m \int_0^{t_1} e^{iB'_0} dt, \quad B'_{t'} \equiv \int_{t'}^{t''} \Delta_m(t) dt. \quad (19)$$

Similarly, for an arbitrarily chosen rear ramp shape we know the desired $\tilde{\alpha}$ and $\tilde{\beta}$ at the end of the flat part t_2 : in first order, $\tilde{\alpha}(t_2) = \tilde{\alpha}(t_f) = -i e^{-i\varphi}$ and

$$\frac{\tilde{\beta}(t_2)}{\tilde{\alpha}(t_2)} = \frac{g_m}{\Delta_m(t_f)} e^{-iB'_0} + i g_m e^{-iB'_0} \int_{t_2}^{t_f} e^{iB'_0} dt. \quad (20)$$

During the flat part of the pulse we can use the two-level approximation with coupling g_m and, essentially, connect the two points on the Bloch sphere corresponding to Eqs. (19) and (20) by a ‘‘Rabi’’ pulse. These points are close to the north and south poles, so the pulse is close to the ideal π pulse; we assume a small constant overshoot $\Delta_m \equiv -D$ with $|D/g_m| \ll 1$ (Fig. 3) and duration $t_2 - t_1 = \pi/\omega_R - \tau$ with $|\tau| \ll \pi/\omega_R$, where $\omega_R \equiv \sqrt{4g_m^2 + D^2}$. Then using the leading-order relation for an almost-perfect π pulse,

$$\frac{\tilde{\beta}(t_2)}{\tilde{\alpha}(t_2)} = \frac{\tilde{\alpha}(t_1)}{\tilde{\beta}(t_1)} + \frac{D}{2g_m} + i g_m \tau, \quad \frac{\tilde{\alpha}(t_2)}{\tilde{\beta}(t_1)} = -i e^{-i\pi D/4g_m}, \quad (21)$$

we obtain the needed pulse parameters D and τ as

$$\frac{D}{2g_m^2} + i\tau = \frac{1}{\Delta_m(0)} + \frac{e^{-iB'_0}}{\Delta_m(t_f)} + i \int_0^{t_1} e^{iB'_0} dt + i e^{-iB'_0} \int_{t_2}^{t_f} e^{iB'_0} dt \quad (22)$$

and also find the resulting phase $\varphi = \pi D/4g_m$.

We have checked numerically the analytical pulse design given by Eqs. (17) and (22). For example, for a piecewise-linear pulse whose front ramp consists of two straight segments (Fig. 3), the error

$$\mathcal{E} = 1 - |\langle 100 | U_{\text{MOVE}} | 010 \rangle|^2 \quad (23)$$

for the analytically designed pulses is found to be below 10^{-3} for typical parameters with $g_m/2\pi = g_b/2\pi = 25$ MHz. As expected, the numerical four-parameter optimization of this pulse shape gives zero error (up to machine accuracy), and the shape of this perfect pulse is close to the analytically designed shape (see Fig. 3).

Experimental pulses for the MOVE operation [7,15,16] are produced by a Gaussian filter and therefore have error-function-shape ramps. We can use the same design idea for such pulses: shaping the front ramp using two parameters (see Fig. 4) takes care of the tail $\tilde{\gamma}(t_f)$ on the bus, for the rear ramp we use any convenient shape, and for the middle part we vary the overshoot frequency and duration to ensure proper population transfer between the qubit and the memory (for such pulses it is natural to define the duration to be between the inflection points of the error-function shapes). We have checked numerically that these four parameters are sufficient to achieve zero error (perfect transfer fidelity $F = 1 - \mathcal{E}$) in the truncated three-element system.

As a further simplification of the MOVE pulse design, let us optimize only two middle-part parameters (overshoot

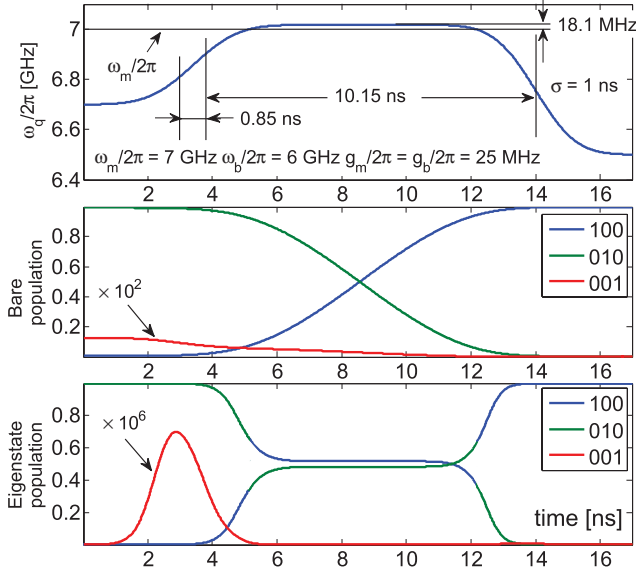


FIG. 4. (Color online) Implementation of the qubit \rightarrow memory MOVE operation in a three-component mqb system using a pulse with error-function-shaped ramps (sum of two time-shifted error functions for the front ramp). Four parameters of the pulse shape (upper panel) are optimized: the time shift and amplitude ratio for the front-ramp error functions, the duration of the middle part of the pulse, and the overshoot magnitude. Error functions are produced by integrating Gaussians with standard deviation $\sigma = 1$ ns; the beginning and end of the pulse are at 3σ from the nearest error-function centers (shown by vertical lines in the upper panel). The middle and lower panels show the time dependence of the level populations in the bare-state basis and comoving eigenbasis. The MOVE error, (23), is zero up to machine accuracy.

and duration), without optimizing the front ramp shape. In this case we cannot ensure the proper tail $\tilde{\gamma}(t_f)$; however, it is small by itself, and therefore the error is not large. Moreover, for sufficiently slow pulses the tail is almost correct automatically because of the adiabatic theorem. It is important to note that the bus is well detuned, $|\Delta_b/g_b| \gg 1$, and then the adiabaticity condition is $|d\Delta_b/dt| \ll |\Delta_b^3/g_b|$, which is well satisfied even by rather fast pulses. To estimate the corresponding error, we consider the two-level system bus-memory during the front ramp and write the differential equation for the variable $y \equiv \gamma/\beta - g_b/\Delta_b$, which describes deviation from the comoving eigenstate. Assuming $|\gamma/\beta| \ll 1$ and $|\dot{\omega}_q \gamma/\beta^2| \ll 1$, we obtain $\dot{y} = i\Delta_b y + g_b \Delta_b^{-2} \dot{\omega}_q$. The tail error at the end of the front ramp is $|y(t_f)|^2$ (note that $|\beta(t_f)| \approx 1$), and it does not change significantly during the rest of the pulse. If this is the major contribution to the MOVE error, then

$$\mathcal{E} = \left| \int_0^{t_1} \frac{g_b}{\Delta_b^2(t)} \dot{\omega}_q(t) \exp(-i\mathcal{A}_0^t) dt \right|^2, \quad (24)$$

where \mathcal{A}_0^t is defined in Eq. (18). Numerical optimization of only the middle part of the pulse (overshoot and duration) confirms that Eq. (24) is a good approximation for the MOVE error in this case. Note that for an error-function ramp obtained by integrating a Gaussian with the standard deviation (time width) σ , the error, (24), decreases exponentially with σ (we

assume a sufficiently long ramp time t_1) and is typically quite small. For example, for $\Delta_b/2\pi$ changing from 0.5 to 1 GHz and $g_b/2\pi = 50$ MHz, the error is below 10^{-4} for $\sigma > 0.5$ ns (for $\sigma > 0.35$ ns if $g_b/2\pi = 25$ MHz).

So far we have only considered the MOVE operation qubit \rightarrow memory. The MOVE operation in the opposite direction, memory \rightarrow qubit, can be designed by using the time-reversed pulse shape. The perfect MOVE operation still requires optimizing four parameters (overshoot and duration of the middle part and the two parameters for the rear ramp), while using only the two parameters for the middle part is sufficient for a high-fidelity MOVE operation.

In designing the MOVE operations between the qubit and the memory, we assumed no quantum information on the bus. The presence of an excitation on the bus makes the previously designed perfect MOVE operation imperfect. We checked numerically that the corresponding error for typical parameters is about 10^{-4} , i.e., quite small. Moreover, a typical RezQu algorithm never needs a MOVE operation between the qubit and the memory with an occupied bus, so the unaccounted MOVE operation errors due to truncation are even much smaller. The analysis in this paper assumes the RWA Hamiltonian, (3), which neglects terms $\propto a_m^\pm \sigma_q^\pm$ and $\propto a_b^\pm \sigma_q^\pm$, which change the number of excitations. We have checked numerically that the addition of these terms into the Hamiltonian leads to negligibly small changes in the system dynamics during the MOVE operations.

Designing MOVE operations between the qubit and the bus is similar to designing MOVE operations between the qubit and the memory, if we consider the truncated three-element system. However, in reality, the situation is more complicated because the bus is coupled with other qubits. Our four-parameter argument in this case does not work, and designing a perfect single-excitation MOVE operation would require $2N + 2$ parameters (for a truncated system with N qubits, one memory, and the bus), which is impractical. However, the occupation of additional qubits is essentially the effect of the tails (if the discussed below problem of level crossing is avoided). Therefore, the desired tails can be obtained automatically by using sufficiently adiabatic ramps in the same way as discussed above (for a MOVE operation qubit \rightarrow bus the front ramp will be important for the tails from both sides, i.e., on the memory and other qubits). In analyzing the dynamics of the tails at other qubits, it is useful to think in terms of eigenstates of a truncated system, which includes the bus and other qubits (while excluding the qubit involved in the MOVE operation). Then the tail error is the occupation of the eigenstates, mainly localized on other qubits. Since the frequencies of the bus and other qubits do not change with time, for the error calculation it is still possible to use Eq. (24), in which Δ_b is replaced with $\omega_q - \omega_{q,k}$ (for the tail on the k th qubit), g_b is replaced with $g_b g_{b,k}/(\omega_{q,k} - \omega_b)$, and \mathcal{A}_0^t is replaced with $\int_0^t [\omega_q(t') - \omega_{q,k}] dt'$, where the subscript k labels an additional qubit. This gives the estimate

$$\mathcal{E} = \left| \int_0^{t_1} \frac{g_b g_{b,k}}{\Delta_{q,k}^2(t)} \dot{\omega}_q(t) e^{-i \int_0^t \Delta_{q,k}(t') dt'} dt \right|^2 \quad (25)$$

of the error due to the tail on the k th qubit for the qubit \rightarrow bus MOVE operation, in which integration is within the front ramp,

$\Delta_{b,k} = \omega_{q,k} - \omega_b$, and $\Delta_{q,k}(t) = \omega_q(t) - \omega_{q,k}$. The formula for the bus \rightarrow qubit MOVE operation is similar, but the integration should be within the rear ramp. The error, (25), should be summed over additional $N - 1$ qubits (index k) and therefore can be significantly larger than in our calculations for a truncated mqb system; however, the error increase is partially compensated by the smaller effective coupling $g_b g_{b,k} / \Delta_{b,k}$. Crudely, we expect errors below 10^{-4} for smooth ramps of a few nanoseconds' duration and $N < 10^2$. We emphasize that this simple solution of the tail problem is possible only when we use eigenstates to represent the logical states.

Another problem which we did not encounter in the analysis of the truncated system is the level crossing with other (empty) qubits during the MOVE operation. A simple estimate of the corresponding error is the following. Effective resonant coupling between the moving qubit and another (k th qubit) via the bus is $g_b g_{b,k} / \Delta_b$, where g_b and $g_{b,k}$ are two qubit-bus couplings and the detuning Δ_b is the same for both qubits at the moment of level crossing. Then using the Landau-Zener formula we can estimate the error (population of the other qubit after crossing) as $\mathcal{E} \simeq 2\pi g_b^2 g_{b,k}^2 / (\Delta_b^2 |\dot{\omega}_q|)$, where $|\dot{\omega}_q|$ is the rate of the qubit frequency change at the crossing. Our numerical calculations show that this estimate works well, though up to a factor of about 2 [when curvature of $\omega_q(t)$ at the point of crossing is significant]. Using this estimate for $g_b/2\pi = g_{b,k}/2\pi = 25$ MHz, $\Delta_b/2\pi = 500$ MHz, and $\dot{\omega}_q/2\pi = 500$ MHz/ns, we obtain the quite significant error of about 10^{-4} . A possible way to compensate this error is by using interference of the Landau-Zener transitions [42] on the qubit return transition. Another solution of the problem is to park empty qubits outside the frequency range between the bus and memories (above 7 GHz in our example). This would make it impossible to cancel the idling error in Eq. (6) by using ‘‘midway parking,’’ but the idling error is still small even without this cancellation [see the estimate following Eq. (8)]. Besides the qubit-qubit level crossings, there are also level crossings between a moving qubit and other memories. This is a higher-order (weaker) process because of three steps between the qubit and memory. The effective coupling with k th memory is then $g_b g_{b,k} g_{m,k} / (\Delta_b \Delta_{m,k})$, and the level crossing error estimate is $\mathcal{E} \simeq 2\pi g_b^2 g_{b,k}^2 g_{m,k}^2 / (\Delta_b^2 \Delta_{m,k}^2 |\dot{\omega}_q|)$.

In this paper we do not analyze two-qubit gates. Our preliminary numerical simulation of the controlled- Z gate has shown the possibility of a high-fidelity gate design (with an error of about 10^{-3} , mainly due to level crossing). However, we have not studied this gate in detail. A detailed analysis of two-qubit gates in the RezQu architecture will be presented elsewhere [36].

V. TUNNELING MEASUREMENT

Finally, let us discuss whether or not using the eigenstates as the logical states presents a problem for measurement. Naively, one may think about a projective measurement of an individual qubit; in this case the logic state 1 would be erroneously measured as 0 with a probability of about $(g_m/\Delta_m)^2 + (g_b/\Delta_b)^2 \sim 10^{-2}$ because the eigenstate spreads to the neighboring memory and bus. This would be a very significant error, and the bare-state representation of logical states would be advantageous. However, this is not actually the

case because any realistic measurement is not instantaneous (not projective). In fact, if a measurement takes longer than $\Delta_{m,b}^{-1}$, then the eigenbasis is better than the bare basis.

As a particular example let us analyze the tunneling measurement of a phase qubit [14] (we expect a similar result for the qubit measurement in the circuit quantum electrodynamics (cQED) setup [26,31]). The bare states $|0\rangle$ and $|1\rangle$ of a phase qubit correspond to the two lowest energy states in a quantum well, and the measurement is performed by lowering the barrier separating the well from essentially a continuum of states [14]. Then state $|1\rangle$ tunnels into the continuum at a significant rate Γ , while the tunneling rate for state $|0\rangle$ is negligible. The event of tunneling is registered by a detector ‘‘click’’ (the detector is a SQUID, which senses the change of magnetic flux produced by the tunneling). In the ideal case, after waiting for a time $t \gg \Gamma^{-1}$ the measurement error is negligibly small (in real experiments the ratio of the two tunneling rates is only $\sim 10^2$, which produces an error of a few percent; however, we neglect this error because, in principle, it can be decreased by transferring the state $|1\rangle$ population to a higher level before the tunneling and, also, because here we are focusing on the effect of tails in the neighboring elements).

In the presence of the memory and bus coupled to the qubit, the logic state 0 still cannot be misidentified, because the tunneling is impossible without an excitation. However, the logic state 1 can be misidentified as 0, when sometimes the expected tunneling does not happen (because part of the excitation is located in the memory and bus). Let us find the probability of this error. For simplicity, we consider a two-component model in which a phase qubit is coupled to its memory resonator only, and restrict the state space to the single-excitation subspace of this mq system. Then the tunneling process can be described by the non-Hermitian Hamiltonian (e.g., [43])

$$H = \begin{bmatrix} \omega_m & g_m \\ g_m & \omega_q - i\Gamma/2 \end{bmatrix}, \quad (26)$$

and the error in measuring the logic state 1 (identifying it as 0 after measurement for time t) is its survival probability

$$\mathcal{E} = |\langle \psi(t) | \psi(t) \rangle|^2, \quad (27)$$

where the initial state is normalized, $|\langle \psi(0) | \psi(0) \rangle|^2 = 1$. Our goal is to compare this error for cases when the initial state is the bare state $|\psi(0)\rangle = |01\rangle$ or the eigenstate $|\psi(0)\rangle = |\tilde{0}\tilde{1}\rangle$ (in this mq notation the qubit state is shown at the second place, and $|\tilde{0}\tilde{1}\rangle$ is the eigenstate before the measurement, i.e., when $\Gamma = 0$).

The solution $|\psi(t)\rangle$ of the time-dependent Schrödinger equation, $i(d/dt)|\psi(t)\rangle = H|\psi(t)\rangle$, is given by the linear combination, $|\psi(t)\rangle = C_m |\tilde{1}\tilde{0}\rangle e^{-iE_m t} + C_q |\tilde{0}\tilde{1}\rangle e^{-iE_q t}$. Here the eigenstate notation with the tilde sign reminds us of a nonzero Γ , the constants $C_{m,q}$ depend on the initial conditions, and $E_{m,q} \equiv \text{Re}(E_{m,q}) - i\Gamma_{m,q}/2$ are the complex eigenenergies, which include the corresponding decay rates Γ_m and Γ_q of the eigenstates located mainly on the memory and the qubit. Diagonalizing Hamiltonian (26) and assuming weak coupling, $g_m \ll \Delta_m$, $g_m \ll \Gamma$, we

find

$$\Gamma_m = \frac{g_m^2 \Gamma}{\Delta_m^2 + (\Gamma/2)^2} \ll \Gamma, \quad \Gamma_q = \Gamma - \Gamma_m \approx \Gamma. \quad (28)$$

For measurement during a sufficiently long time $t \gg \Gamma$, only the $|\tilde{10}\rangle$ term in $|\psi(t)\rangle$ survives, and correspondingly, the error, (27), is $\mathcal{E} = |C_m|^2 e^{-\Gamma_m t}$, where $C_m = \langle \tilde{10} | \psi(0) \rangle$. Thus we obtain

$$\frac{\mathcal{E}_{\text{eigen}}}{\mathcal{E}_{\text{bare}}} = \frac{\Gamma^2}{4\Delta_m^2}, \quad \mathcal{E}_{\text{bare}} = \frac{e^{-\Gamma_m t} g_m^2}{\Delta_m^2 + (\Gamma/2)^2}, \quad (29)$$

for the measurement errors starting either with the eigenstate or with the bare state. Even though both errors decrease with the measurement time t as $e^{-\Gamma_m t}$, the rate Γ_m is small [see Eq. (28)], so for a realistically long measurement we can use $e^{-\Gamma_m t} \approx 1$.

Equation (29) shows that from the measurement point of view it is *advantageous to use the eigenstates* to represent the logical states rather than the bare states if $\Gamma < 2\Delta_m$. For a typical value $\Delta_m/2\pi = 0.5$ GHz, this requires $\Gamma^{-1} > 0.16$ ns, which is always the case.

Figure 5 shows the state dynamics during the tunneling measurement in the bare basis $|\psi(t)\rangle = \alpha(t)|10\rangle + \beta(t)|01\rangle$, starting either with the eigenstate $|0\tilde{1}\rangle$ or with the bare state $|01\rangle$. The oscillations correspond to the beating frequency $\Delta_m/2\pi = 0.5$ GHz. We see that, similarly to the above-analyzed dynamics in the eigenbasis, $|\beta(t)|^2$ becomes exponentially small after $t \gg \Gamma^{-1}$, while $|\alpha(t)|^2$ essentially

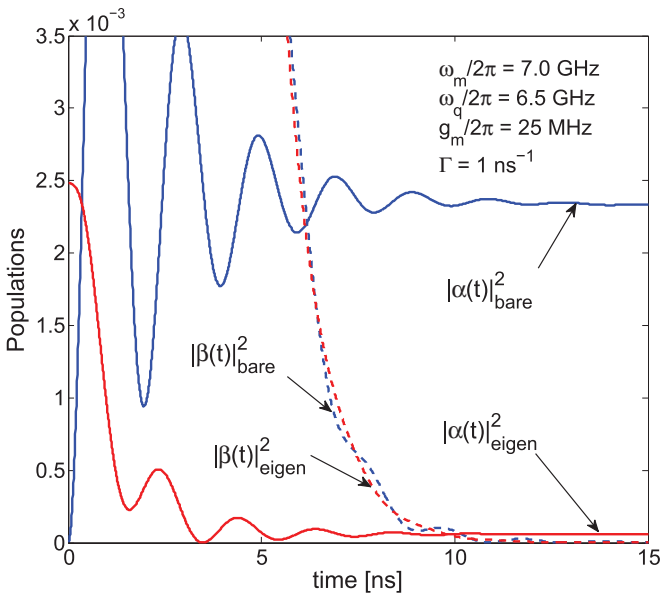


FIG. 5. (Color online) Time dependence of the squared amplitudes $|\alpha|^2$ and $|\beta|^2$ of the mq state $|\psi(t)\rangle = \alpha(t)|10\rangle + \beta(t)|01\rangle$, decaying in the process of tunneling measurement. Blue curves correspond to the system initially prepared in the bare state $|\psi(0)\rangle = |01\rangle$, while for red curves the initial state is the eigenstate $|\psi(0)\rangle = |0\tilde{1}\rangle$. For $t \gg \Gamma^{-1}$ the measurement error, (27), is mainly the residual occupation $|\alpha(t)|^2$ of the memory resonator (solid curves). For the depicted system parameters, $|\alpha_{\text{eigen}}(t)|^2/|\alpha_{\text{bare}}(t)|^2 \approx 0.025$ at $t \gtrsim 10$ ns; i.e., the error of the eigenstate measurement is 40 times smaller than the error of the bare-state measurement.

saturates (decaying at a much lower rate Γ_m). Then for the assumed tunneling rate $\Gamma = 1$ ns $^{-1}$ the ratio of errors $\mathcal{E}_{\text{eigen}}/\mathcal{E}_{\text{bare}} \approx |\alpha_{\text{eigen}}(t)|^2/|\alpha_{\text{bare}}(t)|^2$ (with the subscript denoting the initial state) saturates at approximately the value 0.025 given by Eq. (29).

We emphasize that even though we have only considered the tunneling measurement, the result, (29), for the measurement error is expected to remain crudely valid for the majority of realistic (i.e., “weak”) measurements with a time scale Γ^{-1} . In particular, for the cQED setup we expect that the role of Γ is played (up to a factor) by the ensemble dephasing rate due to measurement.

VI. CONCLUSION

In summary, we have discussed the main ideas of the RezQu architecture and analyzed several error mechanisms, excluding analysis of two-qubit gates. The main advantage of the RezQu architecture is the strong ($> 10^4$ times) reduction in the idling error compared to the conventional bus-based architecture and, also, the effective solution to most of the problems related to spectral crowding. In the absence of decoherence, this makes possible a simple scaling of a RezQu device to ~ 30 qubits without the need for dynamical decoupling. For further scaling the next architectural level of communication between RezQu devices seems to be needed.

We have shown that, instead of using bare states, it is much better to use eigenstates to represent logical states. In this case there is essentially no dynamics in idling (except for the phase errors), which greatly simplifies the modular construction of a quantum algorithm. The logical encoding by eigenstates is also advantageous for single-qubit state generation and measurement. We have presented a simple design for the MOVE operation, which is the most frequent operation in the RezQu architecture. We have shown that a four-parameter optimization is sufficient for designing a perfect MOVE operation in a truncated three-component system. Moreover, optimization of only two experimentally obvious parameters is sufficient for high-fidelity MOVE operations (with errors less than 10^{-4}). While we have not analyzed two-qubit gates, we expect that their design with a similar high fidelity is also possible. Overall, we believe that the RezQu architecture offers a very significant advantage compared to the previously proposed architectures for superconducting qubits, and we believe that this is the practical way to progress toward a medium-scale quantum computing device.

ACKNOWLEDGMENTS

The authors thank Michael Geller, Farid Khalili, Matteo Mariantoni, Leonid Pryadko, and Frank Wilhelm for useful discussions. This work was supported by the IARPA under ARO Grant No. W911NF-10-1-0334.

APPENDIX: DERIVATION OF Ω_{ZZ}

In this Appendix we derive Eq. (6) for $\Omega_{ZZ} = \epsilon_{101} + \epsilon_{000} - \epsilon_{100} - \epsilon_{001}$ in the truncated mqb system. We assume that the couplings g_m and g_b are of the same order, $g_m \sim g_b \sim g$, and do calculations in fourth order in g .

The RWA Hamiltonian, (3), leads to the formation of three subspaces, which do not interact with each other: the ground state $|000\rangle = |000\rangle$ (with zero energy, $\epsilon_{000} = 0$), the single-excitation subspace $\{|100\rangle, |010\rangle, |001\rangle\}$, and the two-excitation subspace $\{|101\rangle, |110\rangle, |011\rangle, |200\rangle, |020\rangle, |002\rangle\}$. It is rather easy to find eigenenergies in the single-excitation subspace; neglecting the direct coupling g_d , in fourth order in g we obtain

$$\epsilon_{100} = \omega_m + \frac{g_m^2}{\Delta_m} - \frac{g_m^4}{\Delta_m^2} + \frac{g_m^2 g_b^2}{\Delta_m^2 (\omega_m - \omega_b)}, \quad (\text{A1})$$

$$\epsilon_{001} = \omega_b - \frac{g_b^2}{\Delta_b} - \frac{g_b^4}{\Delta_b^2} - \frac{g_m^2 g_b^2}{\Delta_b^2 (\omega_m - \omega_b)}. \quad (\text{A2})$$

To find ϵ_{101} , we write the eigenstate $|\overline{101}\rangle$ as a superposition of all elements of the two-excitation subspace,

$$|\overline{101}\rangle = [|101\rangle + \alpha_{110}|110\rangle + \alpha_{011}|011\rangle + \alpha_{200}|200\rangle + \alpha_{020}|020\rangle + \alpha_{002}|002\rangle] / \text{Norm}, \quad (\text{A3})$$

with unimportant normalization. Then the Schrödinger equation $H|\overline{101}\rangle = \epsilon_{101}|\overline{101}\rangle$ (again neglecting g_d) gives six equations:

$$\begin{aligned} (\omega_m + \omega_b) + \alpha_{110}g_b + \alpha_{011}g_m &= \epsilon_{101}, \\ g_b + \alpha_{110}(\omega_m + \omega_q) + (\alpha_{200} + \alpha_{020})g_m\sqrt{2} &= \alpha_{110}\epsilon_{101}, \\ g_m + \alpha_{011}(\omega_q + \omega_b) + (\alpha_{020} + \alpha_{002})g_b\sqrt{2} &= \alpha_{011}\epsilon_{101}, \\ \alpha_{110}g_m\sqrt{2} + \alpha_{200}2\omega_m &= \alpha_{200}\epsilon_{101}, \\ \alpha_{110}g_m\sqrt{2} + \alpha_{011}g_b\sqrt{2} + \alpha_{020}(2\omega_q - \eta) &= \alpha_{020}\epsilon_{101}, \\ \alpha_{011}g_b\sqrt{2} + \alpha_{002}2\omega_b &= \alpha_{002}\epsilon_{101}. \end{aligned} \quad (\text{A4})$$

From the first three of them we obtain

$$\begin{aligned} \epsilon_{101} = \omega_m + \omega_b + \frac{g_m^2 + (\alpha_{020} + \alpha_{002})g_m g_b \sqrt{2}}{\epsilon_{101} - \omega_q - \omega_b} \\ + \frac{g_b^2 + (\alpha_{200} + \alpha_{020})g_m g_b \sqrt{2}}{\epsilon_{101} - \omega_m - \omega_q}, \end{aligned} \quad (\text{A5})$$

which gives ϵ_{101} in fourth order in g if we use second-order ϵ_{101} in the denominators (which is obtained from the same equation using zeroth-order ϵ_{101}) and second-order amplitudes α_{200} , α_{020} , α_{002} . These amplitudes can be found from the last three equations (A4) using the first-order values $\alpha_{110} = -g_b/\Delta_b$,

$\alpha_{011} = g_m/\Delta_m$:

$$\begin{aligned} \alpha_{200} &= \frac{g_m g_b \sqrt{2}}{\Delta_b (\omega_m - \omega_b)}, & \alpha_{002} &= \frac{g_m g_b \sqrt{2}}{\Delta_m (\omega_m - \omega_b)} \\ \alpha_{020} &= \frac{-g_m g_b \sqrt{2}}{\Delta_m \Delta_b} \frac{\omega_m + \omega_b - 2\omega_q}{\omega_m + \omega_b - (2\omega_q - \eta)}. \end{aligned} \quad (\text{A6})$$

Finally, substituting Eq. (A6) into Eq. (A5), and using Eqs. (A1) and (A2), we obtain Eq. (6) for Ω_{ZZ} in fourth order.

The above has been the formal derivation of Eq. (6). Let us also obtain it approximately. Since in a linear system $\Omega_{ZZ} = 0$ (excitations do not interact with each other), a nonzero value can come only from the qubit nonlinearity η . Assuming small η , we can use the first-order perturbation theory in η to find the energy shift of $|101\rangle$ due to the contribution from $|020\rangle$ (occupation of the qubit second level):

$$\Omega_{ZZ} = \delta\epsilon_{101} = -\eta |\alpha_{020}|^2. \quad (\text{A7})$$

To find α_{020} we start with the first-order (in g) eigenstate $|\overline{101}\rangle = |101\rangle - (g_b/\Delta_b)|110\rangle + (g_m/\Delta_m)|011\rangle$ and then obtain the next-order estimate $\alpha_{020} = \sqrt{2}g_m g_b [1/\Delta_b - 1/\Delta_m]/(2\omega_q - \eta - \omega_m - \omega_b)$ [which coincides with Eq. (A6)]. If this estimate is substituted into Eq. (A7), then for Ω_{ZZ} we obtain Eq. (6) with the squared second fraction. However, if in the above formula for α_{020} , we neglect η (as we should for first-order perturbation in η), then we obtain Eq. (6) with the second fraction replaced by 1. One may say that the average between these two results for small η reproduces Eq. (6); however, it is more appropriate to say that this approximation (first order in η) can accurately reproduce only the first fraction in Eq. (6), while the second fraction is beyond the accuracy of the approximation.

A slightly different derivation reproduces Eq. (6) exactly. Instead of using the first-order approximation in η [Eq. (A7)], let us find the change of ϵ_{101} due to its repulsion from ϵ_{020} . Since the effective interaction is $g_{\text{eff}} = \sqrt{2}g_m g_b [1/\Delta_b - 1/\Delta_m]$ (see the above estimate of α_{020}), the repulsion is $\delta\epsilon_{101} = -g_{\text{eff}}^2/(2\omega_q - \eta - \omega_m - \omega_b)$. The difference in this repulsion with vs without nonlinearity η gives $\Omega_{ZZ} = -g_{\text{eff}}^2[(2\omega_q - \eta - \omega_m - \omega_b)^{-1} - (2\omega_q - \omega_m - \omega_b)^{-1}]$, which reproduces Eq. (6).

These simple derivations do not change if we take into account the direct interaction g_d in Hamiltonian (3), which is of second order, $g_d \sim g^2$, because of Eq. (5). Therefore, the fourth-order result, (6), for Ω_{ZZ} should not change either. The rigorous fourth-order calculation shows that $\epsilon_{100} + \epsilon_{001}$ increases by $2g_d g_m g_b / \Delta_m \Delta_b$ due to g_d , but ϵ_{101} increases by the same amount, so these contributions to Ω_{ZZ} cancel each other.

[1] J. Clarke and F. K. Wilhelm, *Nature* **453**, 1031 (2008).
 [2] T. Yamamoto, Yu. A. Pashkin, O. Astafiev, Y. Nakamura, and J. S. Tsai, *Nature* **425**, 941 (2003).
 [3] J. H. Plantenberg, P. C. de Groot, C. J. P. M. Harmans, and J. E. Mooij, *Nature* **447**, 836 (2007).
 [4] M. Steffen, M. Ansmann, R. C. Bialczak, N. Katz, E. Lucero, R. McDermott, M. Neeley, E. M. Weig, A. N. Cleland, and J. M. Martinis, *Science* **313**, 1423 (2006).

[5] L. DiCarlo, J. M. Chow, J. M. Gambetta, L. S. Bishop, B. R. Johnson, D. I. Schuster, J. Majer, A. Blais, L. Frunzio, S. M. Girvin, and R. J. Schoelkopf, *Nature* **460**, 240 (2009).
 [6] L. DiCarlo, M. D. Reed, L. Sun, B. R. Johnson, J. M. Chow, J. M. Gambetta, L. Frunzio, S. M. Girvin, M. H. Devoret, and R. J. Schoelkopf, *Nature* **467**, 574 (2010).

- [7] M. Mariantoni, H. Wang, T. Yamamoto, M. Neeley, R. C. Bialczak, Y. Chen, M. Lenander, Erik Lucero, A. D. O'Connell, D. Sank, M. Weides, J. Wenner, Y. Yin, J. Zhao, A. N. Korotkov, A. N. Cleland, and J. M. Martinis, *Science* **334**, 61 (2011).
- [8] T. Hime, P. A. Reichardt, B. L. T. Plourde, T. L. Robertson, C. E. Wu, A. V. Ustinov, and J. Clarke, *Science* **314**, 1427 (2006).
- [9] F. Altomare, J. I. Park, K. Cicak, M. A. Sillanpää, M. S. Allman, D. Li, A. Sirois, J. A. Strong, J. D. Whittaker, and R. W. Simmonds, *Nature Phys.* **6**, 777 (2010).
- [10] J. Bylander, S. Gustavsson, F. Yan, F. Yoshihara, K. Harrabi, G. Fitch, D. G. Cory, Y. Nakamura, J. S. Tsai, and W. D. Oliver, *Nature Phys.* **7**, 565 (2011).
- [11] F. Mallet, F. R. Ong, A. Palacios-Laloy, F. Nguyen, P. Bertet, D. Vion, and D. Esteve, *Nature Phys.* **5**, 791 (2009).
- [12] R. Vijay, D. H. Slichter, and I. Siddiqi, *Phys. Rev. Lett.* **106**, 110502 (2011).
- [13] For a high-level architecture solution, see D. P. DiVincenzo, *Phys. Scripta T* **137**, 014020 (2009).
- [14] J. M. Martinis, *Quant. Inform. Proc.* **8**, 81 (2009).
- [15] H. Wang, M. Mariantoni, R. C. Bialczak, M. Lenander, E. Lucero, M. Neeley, A. D. O'Connell, D. Sank, M. Weides, J. Wenner, T. Yamamoto, Y. Yin, J. Zhao, J. M. Martinis, and A. N. Cleland, *Phys. Rev. Lett.* **106**, 060401 (2011).
- [16] M. Mariantoni, H. Wang, R. C. Bialczak, M. Lenander, E. Lucero, M. Neeley, A. D. O'Connell, D. Sank, M. Weides, J. Wenner, T. Yamamoto, Y. Yin, J. Zhao, J. M. Martinis, and A. N. Cleland, *Nature Phys.* **7**, 287 (2011).
- [17] S. T. Merkel and F. K. Wilhelm, *New J. Phys.* **12**, 093036 (2010).
- [18] F. W. Strauch, P. R. Johnson, A. J. Dragt, C. J. Lobb, J. R. Anderson, and F. C. Wellstood, *Phys. Rev. Lett.* **91**, 167005 (2003).
- [19] G. Haack, F. Helmer, M. Mariantoni, F. Marquardt, and E. Solano, *Phys. Rev. B* **82**, 024514 (2010).
- [20] T. Yamamoto, M. Neeley, E. Lucero, R. C. Bialczak, J. Kelly, M. Lenander, M. Mariantoni, A. D. O'Connell, D. Sank, H. Wang, M. Weides, J. Wenner, Y. Yin, A. N. Cleland, and J. M. Martinis, *Phys. Rev. B* **82**, 184515 (2010).
- [21] A. O. Niskanen, K. Harrabi, F. Yoshihara, Y. Nakamura, S. Lloyd, and J. S. Tsai, *Science* **316**, 723 (2007).
- [22] R. C. Bialczak, M. Ansmann, M. Hofheinz, E. Lucero, M. Neeley, A. D. O'Connell, D. Sank, H. Wang, J. Wenner, M. Steffen, A. N. Cleland, and J. M. Martinis, *Nature Phys.* **6**, 409 (2010).
- [23] S.-L. Zhu, Z. D. Wang, and K. Yang, *Phys. Rev. A* **68**, 034303 (2003).
- [24] A. Blais, A. M. van den Brink, and A. M. Zagoskin, *Phys. Rev. Lett.* **90**, 127901 (2003).
- [25] X. Zhou, M. Wulf, Z. Zhou, G. Guo, and M. J. Feldman, *Phys. Rev. A* **69**, 030301 (2004).
- [26] A. Blais, R.-S. Huang, A. Wallraff, S. M. Girvin, and R. J. Schoelkopf, *Phys. Rev. A* **69**, 062320 (2004).
- [27] A. N. Cleland and M. R. Geller, *Phys. Rev. Lett.* **93**, 070501 (2004).
- [28] A. Blais, J. Gambetta, A. Wallraff, D. I. Schuster, S. M. Girvin, M. H. Devoret, and R. J. Schoelkopf, *Phys. Rev. A* **75**, 032329 (2007).
- [29] J. Koch, T. M. Yu, J. Gambetta, A. A. Houck, D. I. Schuster, J. Majer, A. Blais, M. H. Devoret, S. M. Girvin, and R. J. Schoelkopf, *Phys. Rev. A* **76**, 042319 (2007).
- [30] J. Majer, J. M. Chow, J. M. Gambetta, Jens Koch, B. R. Johnson, J. A. Schreier, L. Frunzio, D. I. Schuster, A. A. Houck, A. Wallraff, A. Blais, M. H. Devoret, S. M. Girvin, and R. J. Schoelkopf, *Nature* **449**, 443 (2007).
- [31] R. J. Schoelkopf and S. M. Girvin, *Nature* **451**, 664 (2008).
- [32] J. Q. You, and F. Nori, *Nature* **474**, 589 (2011).
- [33] E. J. Pritchett and M. R. Geller, *Phys. Rev. A* **72**, 010301(R) (2005).
- [34] M. A. Sillanpää, J. I. Park, and R. W. Simmonds, *Nature* **449**, 438 (2007).
- [35] B. R. Johnson, M. D. Reed, A. A. Houck, D. I. Schuster, L. S. Bishop, E. Ginossar, J. M. Gambetta, L. DiCarlo, L. Frunzio, S. M. Girvin, and R. J. Schoelkopf, *Nature Phys.* **6**, 663 (2010).
- [36] J. Ghosh *et al.* (in preparation, 2011).
- [37] M. A. Nielsen and I. L. Chuang, *Quantum Computation and Quantum Information* (Cambridge University Press, Cambridge, UK, 2000).
- [38] M. Boissonneault, J. M. Gambetta, and A. Blais, *Phys. Rev. A* **79**, 013819 (2009).
- [39] R. A. Pinto, A. N. Korotkov, M. R. Geller, V. S. Shumeiko, and J. M. Martinis, *Phys. Rev. B* **82**, 104522 (2010).
- [40] M. Hofheinz, H. Wang, M. Ansmann, R. C. Bialczak, Erik Lucero, M. Neeley, A. D. O'Connell, D. Sank, J. Wenner, J. M. Martinis, and A. N. Cleland, *Nature* **459**, 546 (2009).
- [41] L. P. Pryadko and A. N. Korotkov (unpublished).
- [42] W. D. Oliver, Yang Yu, J. C. Lee, K. K. Berggren, L. S. Levitov, and T. P. Orlando, *Science* **310**, 1653 (2005); M. Sillanpää, T. Lehtinen, A. Paila, Yu. Makhlin, and P. Hakonen, *Phys. Rev. Lett.* **96**, 187002 (2006).
- [43] K. Gottfried and V. F. Weisskopf, *Concepts of Particle Physics*, Vol. I (Oxford University Press, New York, 1984), p. 151.